물리탐사
Vol. 5, No. 3, 2002, p. 157~168

Recovery of Lithospheric Magnetic Components in the Satellite Magnetometer Observations of East Asia

Jeong Woo Kim[1)]

인공위성 자력계에서 관측된 동아시아 암권의 지자기이상

김정우[1)]

Abstract : Improved procedures were implemented in the production of the lithospheric magnetic anomaly map from Magsat satellite magnetometer data of East Asia between 90°E-150°E and 10°S-50°N. Procedures included more effective selection of the dusk and dawn tracks, ring current correction, and separation of core field and external field effects. External field reductions included an ionospheric correction and pass-by-pass correlation analysis. Track-line noise effects were reduced by spectral reconstruction of the dusk and dawn data sets. The total field magnetic anomalies were differentially-reduced-to-the-pole to minimize distortions between satellite magnetic anomalies and their geological sources caused by corefield variations over the study area. Aeromagnetic anomalies were correlated with Magsat magnetic anomalies at the satellite altitude to test the lithospheric veracity of anomalies in these two data sets. The aeromagnetic anomalies were low-pass filtered to eliminate high frequency components that may not be shown at the satellite altitude. Although the two maps have a low CC of 0.243, there are many features that are directly correlated (peak-to-peak and trough-to-trough). The low CC between the two maps was generated by the combination of directly- and inversely-correlative anomaly features between them. It is very difficult to discriminate directly, inversely, and nully correlative features in these two anomaly maps because features are complicatedly correlated due to the depth and superposition of the anomaly sources. In general, the lithospheric magnetic components were recovered successfully from satellite magnetometer observations and correlated well with aeromagnetic anomalies in the study area.

Keywords : Magsat, satellite magnetic anomalies, East Asia, lithospheric components

요 약 : Magsat 인공위성의 자력계로부터 관측된 동아시아 (동경90도-50도, 남위10도-북위50도) 암권의 자기이상을 추출하기 위한 연구를 수행하였다. 이를 위해 ring current correction, ionospheric correction, pass-by-pass correlation 등을 실시하였고, 위성트랙 잡음을 효율적으로 제거하기 위한 spectral reconstruction을 실시하였다. 최종적으로 추출된 자기이상의 신뢰도를 검증하기 위해 항공자기이상과 대비하였고, 이를 위해 항공자기이상에 low-pass 필터를 적용하여 인공위성 고도에서 관측 불가능한 고주파성분을 제거하였다. 결과적으로 위성자기이상과 항공자기이상은 0.243의 비교적 낮은 상관관계를 보이나 연구지역내 많은 부분에서 양(+)의 상관관계를 갖고 있음이 밝혀졌다. 일반적으로 낮은 상관계수는 각 주파수별 성분의 양과 음의 상관계수가 혼합되어 나타나며, 따라서 본 연구와 같은 포텐셜이상의 경우에는 이상체의 심도 및 누중 때문에 양과 음의 상관관계를 갖는 이상체를 분류하는 것이 매우 어렵다. 본 연구에서는 인공위성 자력계 관측값으로부터 연구지역 암권의 자기이상을 성공적으로 추출하였으며 항공자기이상과도 양호한 상관관계를 갖고 있음이 밝혀졌다.

주요어 : Magsat, 인공위성 지자기이상, 동아시아, 암권 자기이상

Introduction

Airborne magnetic field surveys (at altitudes up to of 5 km above the Earth's surface) have been carried out since 1950's to conduct various types of geophysical and geological investigations. In the early 1970's, satellite magnetic observations were first found to provide the long wavelength lithospheric components that are difficult to map by airborne surveys (Regan *et al.*, 1975: Potemra *et al.*, 1980). Recognizing the utility of satellites for mapping regional magnetic anomalies of the lithosphere, NASA launched the Magsat satellite as the first mission specifically designed for map-

*2002년 6월 27일 접수

1) 세종대학교 지구정보과학과/지구정보연구소(Dept. of Geoinformation Sciences and Research Inst. of Geoinformatics & Geophysics, Sejong University, 98 Kunja-dong, Kwangjin-ku, Seoul, 143-747, Korea. (jwkim@sejong.ac.kr)

ping lithomagnetic anomalies. Since the Magsat mission, Danish/French/Nasa's Ø rsted and German Champ satellites are currently orbiting the Earth to map regional vector and scalar geomagnetic anomalies.

Magsat obtained vector measurements of the near-earth geomagnetic field (Langel, 1985). Although it is very difficult and complicated to reduce the satellite magnetic anomaly data for lithospheric components, these data can provide useful constraints for modeling regional features of the lithosphere, especially when combined with near-surface magnetic and concomitant geological and geophysical observations.

Since regional variations of lithospheric magnetization (*i.e.* magnetic anomalies of lithosphere) are uniquely reflected in atellite magnetic anomalies, satellite-altitude magnetic anomalies in the East Asia region will show good correlation with the geologic and tectonic features. These variations are related to changes in lithology, thermal property, and lithospheric thickness, which resulted from the tectonic evolution of the lithosphere (Wasilewsky *et al.*, 1979: von Frese *et al.*, 1989). In other words, analysis of satellite magnetic anomalies can provide unique and important information on geology and tectonics of the lithosphere.

Accurate recovery of the lithospheric magnetic anomaly is necessary to better understand the lithospheric structures related to the anomaly features. To obtain a lithyospheric magnetic field over Asia (0°-120°E, 10°-50°N), Achache *et al.* (1987) applied a spherical harmonic model up to degree and order 13 to eliminate the corefield components generated by the self-exciting dynamo in the Earths core. They also reduced the data for ionospheric field effects (or equatorial electrojet effects) by fitting and removing an 8th-order polynomial to each orbital data profile. They produced 2°-by-2° averaged dusk and dawn data of the vertical component of the magnetic anomalies that they continued downward to the Earth's surface for geologic analysis. Anomaly discrepancies, however, remained between the dusk and dawn maps, such as observed for northern China, that can impact geological interpretation greatly. A scalar magnetic anomaly map for East Asia was also produced by Arkani-Hamed *et al.* (1988). They removed wavelengths shorter than ~540 km that they considered non-lithospheric magnetic components, as well as wavelengths longer than ~2,300 km that were suggested to relate to the external field effects. However, they noted that non-lithospheric components may not be completely removed by the use of a band-pass filter because magnetic anomalies smaller than 2 nT were poorly correlated between the band-pass filtered dusk and dawn data sets.

Separation of corefield and lithospheric magnetic components in the satellite magnetometer observations is still not well understood. Langel and Estes (1985) suggested that magnetic features of degree less than 13 are dominated by the corefield, whereas features of degree higher than 15 are due mostly to lithospheric effects. Meyer *et al.* (1985) found from the spatial energy density spectrum of the modeled vertical (*i.e.*, Z) component satellite lithospheric magnetic anomalies for North and Central America that significant lithospheric components may exist to degree 4 at least. Cain *et al.* (1989) found that the geomagnetic spectrum for IGRF 1980 displayed a dramatic change at degree 15, which may reflect the spectral transition between core and lithospheric components. Arkani-Hamed and Strangway (1986) analyzed the spherical harmonic expansion of Magsat total magnetic field anomalies and found little correlation in ascending and descending data sets between degrees 15 and 17. Hence, they used degrees greater than or equal to 17 to represent the magnetic anomalies of the lithosphere in their study.

In this paper, an advanced approach was considered to accurately separate core and lithospheric field components in satellite magnetic data. In particular, enhanced core and external field separation procedures using wavenumber correlation analysis (WCA) (von Frese *et al.*, 1997a) and quadrant-swapping method (Kim *et al.*, 1998) will be discussed to produce an improved lithospheric magnetic anomaly map for the East Asia between 90°E-150°E and 10°S-50°N.

To test the veracity of the developed procedures, the satellite-derived anomalies will be compared with the aeromagnetic anomalies by Geological Survey of Japan and CCOP (1996). It is because the effective lithospheric analysis requires comparing satellite elevation signals with related signals at sea level or airborne altitudes.

Data Processing

The data reduction procedures for separating core, external and lithospheric field components are described here. An outline for implementing these procedures on Magsat magnetometer data is displayed as a flow chart in Fig. 1.

Pre-Processing

Geomagnetic field components of the global Earth gathered by the Magsat mission were processed into 1/16 second

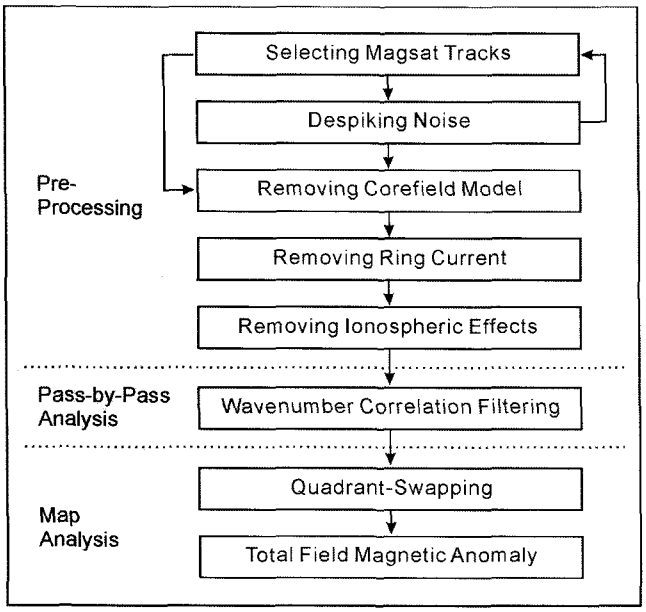

Fig. 1. Workstream of Magsat satellite magnetometer data processing.

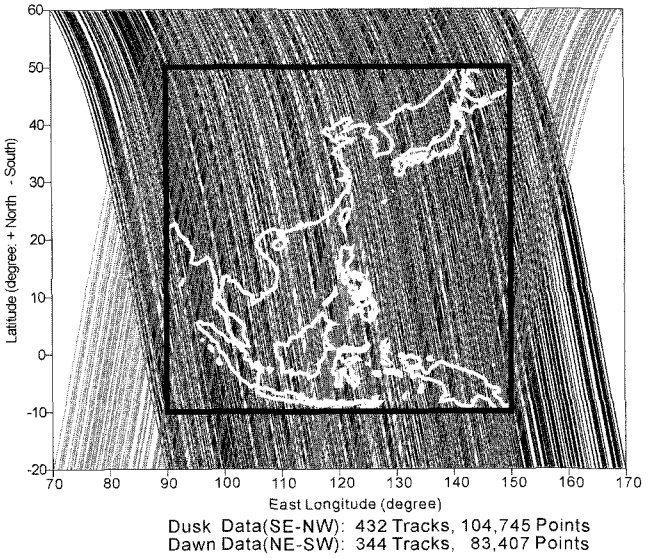

Fig. 2. Magsat orbit distribution with the study area highlighted. Ascending (dusk) orbits have a SE to NW trend, whereas the descending (dawn) orbits have a NE to SW trend. Total numbers of tracks (data points) for dusk and dawn data sets are 432 (104,745) and 344 (83,407), respectively.

data and stored in Chronicle tapes (Langel *et al.*, 1981). The data density on these tapes was too large to be manageable for most studies. Therefore, averages of every 80 data points were recorded on the Investigator-B tapes, which resulted in a data density of one point every 5 seconds (Langel *et al.*, 1981). The total size of all the records contained in these tapes is about 180.6 MB. Only data for an extended study area (70°E-170°E, 20°S-50°N) are extracted from the tapes and analyzed. To maintain good coverage and minimize edge effects, the extended area will be considered for processing the satellite orbits.

Of the more than 3000 orbital tracks on the Investigator-B tapes, 776 orbital tracks were selected. These tracks were grouped into dusk and dawn data sets, based on their local magnetic times. This partitioning is essential for performing 1-D Wavenumber Correlation Analysis (WCA) (von Frese *et al.*, 1997a: Kim *et al.*, 2000). Also, this enhances the perception of external fields in the Magsat maps that were compiled according to different local times for more effective extraction of lithospheric anomaly (Arkani-Hamed and Strangway, 1986: Alsdorf *et al.*, 1994a: Kim, 1996). The dusk and dawn data are processed independently and then merged to produce a total field magnetic anomaly map.

The orbital coverages for dusk and dawn local magnetic times are shown in Fig. 2 wherein the study area is also displayed. The orbital data are reformatted from time to spatial (longitude) orientation. Data spikes are removed by a despiking algorithm by Alsdorf *et al.* (1994a). The minimum numbers of points for each track are evaluated to identify and eliminate short tracks. Instead of using standard geomagnetic indices (*e.g.*, K_p, A_m) to evaluate data quality as has been done in previous studies (*e.g.*, Langel *et al.*, 1981: Arkani-Hamed and Strangway, 1986), the data were screened in terms of their statistical variances and average elevations along the orbital tracks. For East Asia, tracks with variances higher than 100 nT^2 were removed.

Minimizing elevation variations in the data set will facilitate the application of later procedures such as least-squares collocation for gridding the data at constant elevation (Goyal *et al.*, 1990). In general, the elevation of Magsat tracks ranges between 220 km and 580 km. In this study, tracks with elevations between 325 km to 450 km are selected for producing a Magsat anomaly map of the study area. For processing, there are 432 dusk tracks and 344 dawn tracks available, as shown in Fig. 2. Total numbers of data points are 104,745 and 83,407 for dusk and dawn data sets, respectively.

In the previous studies by Arkani-Hamed and Strangway (1986) and Alsdorf *et al.* (1994a, 1994b), the observations were interpolated at 1/3 of a degree in latitude along the orbital track, which was roughly the same spacing of the data over regions of low latitude. However, such interpolations are not suitable for mid to high latitude regions where

this sampling interval would undersample the data, resulting in the distortions when the data are analyzed in the wavenumber domain. Accordingly, for this study, a densifying cophasing technique was implemented that better honored the original data coverage and anomaly detail. The procedures of Kim (1996) for preparing adjacent tracks of satellite altimetry data for WCA were adapted for Magsat data processing. With these procedures, a sampling interval was determined in spherical coordinates so that the number of uniformly-spaced estimates are not less than the number of original data points. The use of these procedures helps to preserve anomaly detail, and they provide sample points that are orthogonal to each other across each pair of neighboring tracks. Hence, in the coordinate reference frame of each pair of neighboring orbits, the resampled data estimates are coregistered for optimal spectral correlation processing.

Corefield and External Field Reductions

Langel and Estes (1985) found that the Magsat power spectrum showed a pronounced change in slope at degree and order 13. They suggested that the corefield dominates the components below degree 13. The lithospheric and corefield effects have spectral components that are intermixed between degrees 13 and 15. For the processing, the components to degree 12 of the corefield model GSFC12/83 were taken to be dominated by corefield effects. Only these components were removed in producing total field scalar anomalies that also contained residual corefield components above degree 12. Fig. 3 shows the corefield to degree and order 12 at 400 km elevation that was removed from the Magsat observations. Attributes listed for the map include the Amplitude Range, AR of (minimum, maximum), the Amplitude Mean, AM, and the Amplitude Standard Deviation, ASD.

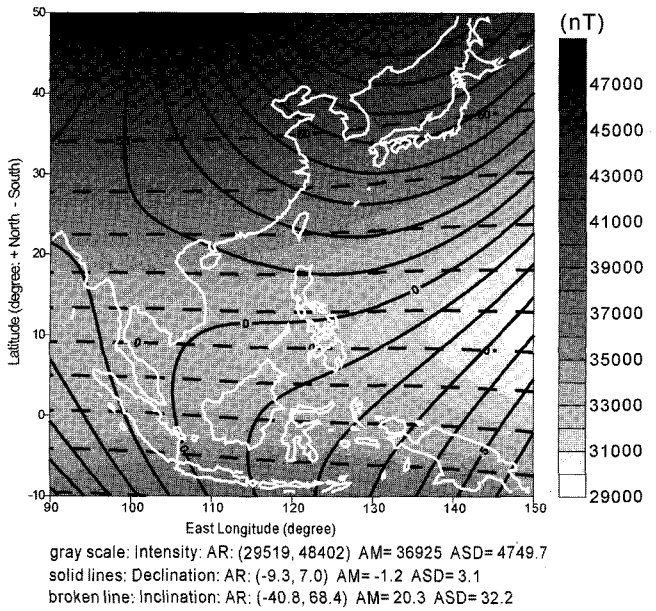

Fig. 3. Corefield to degree and order 12 at 400 km above sea level. Gray scale is for the intensity of corefield (nT), and solid and broken lines denote declination and inclination (degrees), respectively. Attributes listed for the map include the Amplitude Range, AR of (minimum, maximum), the Amplitude Mean, AM, and the Amplitude Standard Deviation, ASD.

At satellite altitude, effects due to the equatorial ring current (Langel, 1971) can cause significant distortions of lithospheric anomalies over the study area. To minimize this effect in the Magsat data, the algorithm by Langel *et al.* (1981) was used. The ring current effect was subtracted out of the total field point-by-point along each track. Fig. 4A and 4B show the dusk and dawn ring core effects and 4C and 4D shows residual anomalies after correcting for the ring current effects, respectively. They are gridded at a common elevation of 400 km, using the least-squares collocation method of Goyal *et al.* (1990). The correlation coefficient (CC) of Fig. 4C and 4D is 0.83.

The induced magnetic field in the ionosphere generates a strong east-west trend that ignores major features of the crustal lithosphere. These ionospheric effects, which can severely impact geological interpretation, are much more significant near the equator than at high latitudes because the magnetic field is horizontal or nearly horizontal in this region (Ravat and Hinze, 1993). Thus, the removal of equatorial ionospheric effects becomes very important for isolating the lithospheric components in satellite magnetic data.

Different methods have been proposed to calculate ionospheric effects. Earlier studies mostly focused on simply finding the best fitting lower order function to subtract out of each orbital data track (Mayhew, 1985: Regan *et al.*, 1975). Yanagisawa and Kono (1985) modeled the ionospheric field as a function of position and local magnetic time. After removing main field and external field effects, the residual anomaly should contain only lithospheric and ionospheric components. Averaging the residual field in longitude and latitude bins, the lithospheric component is attenuated assuming that geologic signals are not correlated in longitude and latitude. The average is called the mean ionospheric field (MIF), which, when subtracted from the residual field, should yield the lithomagnetic anomalies. However, the resulting lithospheric anomaly map that they produced

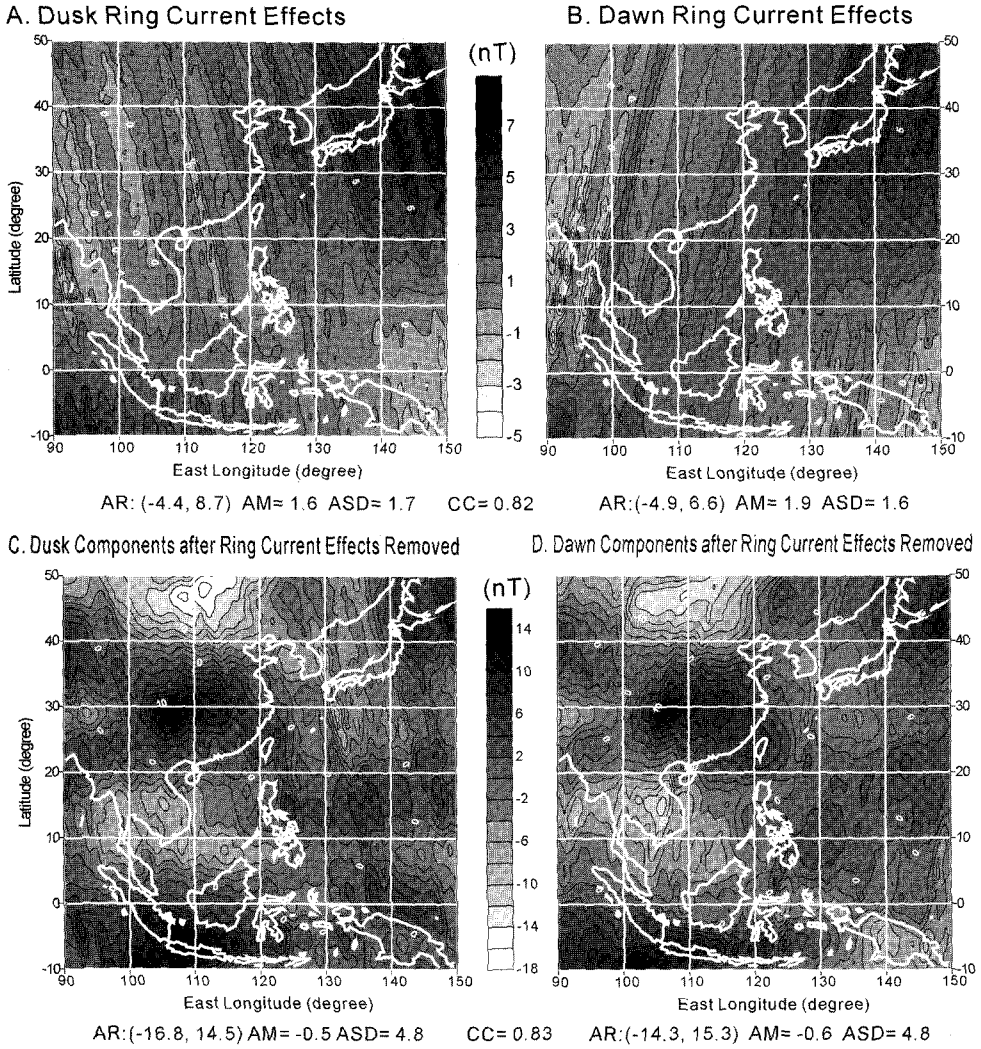

Fig. 4. Ring current effects of dusk and dawn data sets (A, B) and magnetic anomalies after ring currents removed (C, D).

was at a 5°-by-5° resolution, so that the Magsat magnetic anomaly detail was inordinately reduced (Cohen and Achache, 1990).

To improve the resolution of Magsat anomalies, Cohen and Achache (1990) tried another approach that calculates the mean equatorial anomaly (MEA) by averaging all profiles at constant dip latitude for each vector component of the dusk and dawn data sets. The differences between dawn and dusk MEAs are taken to be ionospheric effects that are subtracted from both dusk and dawn data. However, the ionospheric effects are not well represented in cases where dusk and dawn data sets are similar because the common features in the dusk and dawn averages that originated from ionospheric effects will be removed by taking the difference (Ravat and Hinze, 1993).

Instead of obtaining an average for each component, Ravat and Hinze (1993) averaged the total magnetic field as a function of dip latitude to obtain dip-latitude averages for the dusk and dawn data. They investigated the variability of the dusk and dawn averages in equatorial excursions by longitude, altitude, and monthly interval. Their analysis indicated that the MIF (Yanagisawa and Kono, 1985) is more meaningful than MEA (Cohen and Achache, 1990) because dusk dip-latitude averages are more compatible with the daytime POGO averages. Analysis of longitudinal variations indicates that the correction must be applied to both dusk and dawn data. Their analysis also indicated that although the variation of dip-latitude averages attenuates with altitude, the correction is much more complicated than assigning a predetermined attenuation function. Hence, Ravat and Hinze (1993) removed least squares fits of dip-latitude averages (Cohen and Achache, 1990) from each Magsat profile to estimate lithospheric components. However, seasonal variations for the dusk dip-latitude averages in the African sector

are not well understood presently and require additional study to more fully account for their effects.

Thus, by investigating the longitudinal, altitude, and seasonal variability of the equatorial excursion of the dusk and dawn dip-latitude averages, Ravat and Hinze (1993) obtained an improved procedure for reducing the ionospheric effect using finer (1°) spacing of dip-latitude averages and a least-squares fit of the mean dip-latitude averages to account for altitude variations. This method was applied in this paper to estimate the ionospheric effects for the Magsat dusk (Fig. 5A) and dawn (5B) data which reflect relatively strong EW trends. The dusk and dawn maps after removing ionospheric corrections are displayed in Fig. 5C and 5D. The CC between Fig. 5C and 5D has been increased by about 2.4% from 0.83 to 0.85.

Pass-by-Pass Analysis

To remove further external field effects in the data, wavenumber correlation analysis (WCA) is applied between subparallel neighboring tracks. As is well known, external fields vary with time and space, whereas lithospheric anomalies are static over the time span of the Magsat mission. Thus, the lithospheric anomalies for two neighboring tracks should be highly correlated where the distance between the tracks is small compared to their altitudes. On the other hand, non-correlative components may be related to external field effects that are dynamic in space and time and other non-lithospheric components.

The spectral correlation technique developed by von Frese *et al.* (1997a) compares two signals, X and Y, for their correlation spectrum in the wavenumber domain. Their transforms are represented by $\underline{X}$ and $\underline{Y}$. The correlation coefficient (CC_k) between two k-th wavenumber components with phase difference $\Delta\theta_k$ is given by $\mathbf{CC}_k = \cos(\Delta\theta_k)$.

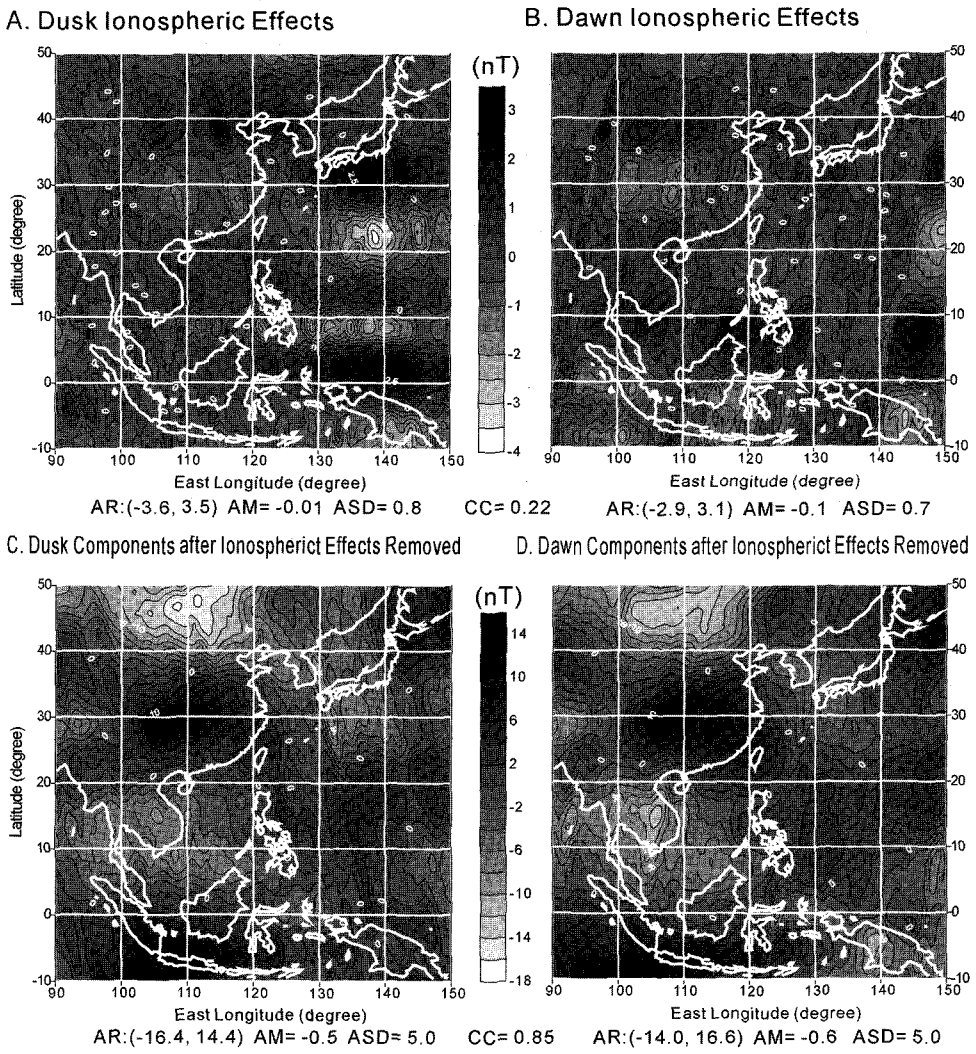

Fig. 5. Equatorial electrojet effects of dusk and dawn data sets (A, B) and magnetic anomalies after ionospheric corrections (C, D).

A 1-dimensional spectral correlation is applied to the pass and its neighboring east and west passes (*i.e.*, pass-by-pass Analysis in Fig. 1) to extract the remaining external field components (Kim, 1996). To facilitate taking the FFT, data points in the neighboring tracks are represented by a common number of interpolated points that is a power of 2. To reduce the distortion in spectral analysis, the neighboring tracks are geodetically cophased (Kim, 1996) so that the tracks may be resampled for data points that are orthogonal to each other. The correlation spectrum between the resampled tracks is computed for each pair of neighboring tracks in the dusk and dawn data sets.

The choice of cut-off CC is very important for performing optimal WCA in the data processing. The power and the frequencies of the filtered output signals depend significantly upon the choice of cut-off CC. The input CCs between two sub-parallel tracks are dictated by the signal similarities between two tracks, and, therefore, it is necessary to study the input CCs and tracks before deciding on a cut-off CC. Unlike the satellite radar altimeter data (Kim, 1996), the CCs for the Magsat data orbits are relatively poor, even after removing ring current effects, corefield model (Kim, 1996). This indicates that non-lithospheric effects such as external fields variations and other noise may be present in the data and must be eliminated. For this study, a cut-off CC of 0.4 was selected to retain substantial power in the output after variations in the output power with the CC are calculated at increments of 0.1 for a cut-off. A cut-off CC of 0.4 is consistent with previous experiences in processing the Magsat data for geological studies (Kim *et al.*, 1992, 1994, 1995a, 1995b). After the filtering, the common components were averaged and assigned to the middle of the two neighboring tracks that is very close to the original distances between two consecutive observation points along a track. The point-by-point averages of filtered components were then located mid-way between the two tracks.

Maps in Fig. 6A and 6B display the dusk and dawn maps after the pass-by-pass correlation analysis (*i.e.*, 1-D WCA). They are gridded at a common elevation of 400 km for further analysis using the least-squares collocation method of Goyal *et al.* (1990).

Map-by-Map Analysis

Efforts to enhance correlations between dusk and dawn data further focus on reducing track noise between the two data sets. To reduce the Magsat data for these effects, a quadrant-swapping method is adapted from satellite altimetry data processing (Kim *et al.*, 1998).

As simplified in Fig. 7, the noise and Magsat track line directions both subtend an angle of q counterclockwise from the reference direction or the Y-axis in the upper panel. The λ(X) and λ(Y) wavelength components of track-line noise in the X- and Y-directions, respectively, are related to θ by (tan $\theta = \lambda(X)/\lambda(Y)$). The spectral components of this noise occur in the quadrants that are orthogonal to the direction of the lines, because wavenumbers, k, are inversely related to the wavelengths, λ, by ($k = 2\pi/\lambda$), so that (tan $\theta = \lambda(X)/\lambda(Y) = k(Y)/k(X)$). Accordingly, spectral distortions due to track-line noise are limited only to a single pair of symmetric quadrants as shown in Fig. 6C and 6D, and the other orthogonal pair of symmetric quadrants is essentially uncontaminated (Kim *et al.*, 1998).

To suppress track-line noise in the dusk data set, for example, a fan filter might be designed to attenuate the contaminated wavenumber components. However, a better approach is possible because a pair of maps at different line azimuths (*i.e.* duck and dawn maps) exists. In this case, the noise-contaminated quadrants of dusk map in Fig. 6 turned out to be orthogonal to the contaminated quadrants of the dawn map's power spectrum. Hence, the result may be improved by the use of a fan reject filter by simply exchanging contaminated wavenumber components for uncontaminated wavenumber components between the two spectra. Inverse transforming the reconstructed spectra will yield two maps that might be combined to enhance further the signal-to-noise ratio of the survey.

Simple differencing of the spectra will highlight the contaminated wavenumber components for modification. However, these spectral differences can be difficult to interpret in practice because they often reflect additional map distortions, such as the effects from disparate sources of error between the two data sets or the non-linearity of survey lines, etc. The non-linearity of the orbital tracks is a further complication that becomes increasingly severe as the scale and latitude of the survey region increases. For example, the reference angle, θ, in Fig. 7 and satellite's azimuth, α, are related by ($\theta = 360^\circ - \alpha$). However, from Clairaut's equation, $\alpha(\phi)$ equals to $\sin^{-1}$ (cos I / cos ϕ), where ϕ denotes latitude and I is the satellite's inclination. Hence, by the equation, the Magsat satellite's azimuth varies between 79.0° and 82.9° with latitude over the study area.

In Fig. 6C and 6D, errors and non-linearity result in a dif-

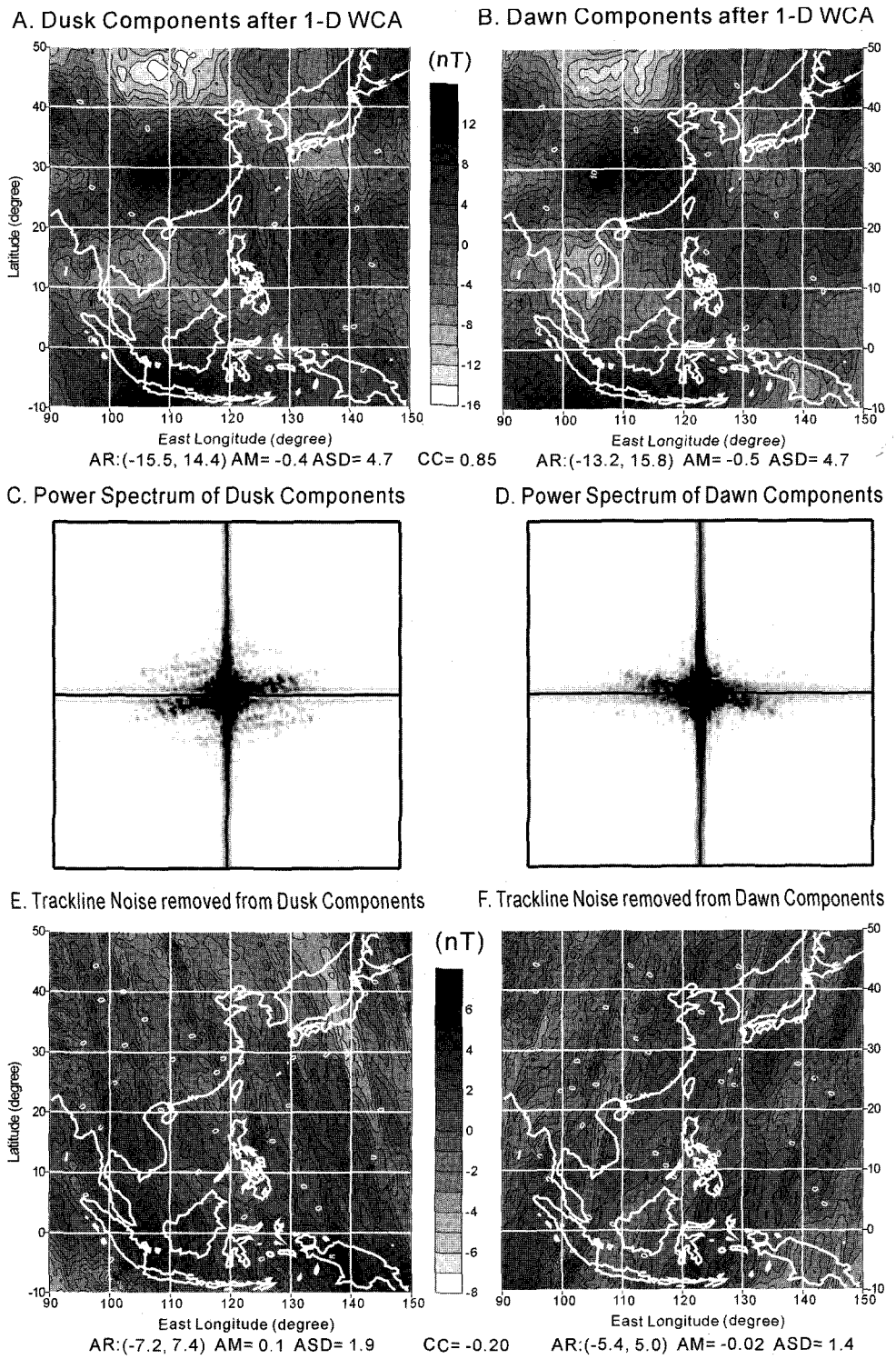

Fig. 6. 1-D wavenumber correlation filtered dusk and dawn magnetic anomalies (A, B) and their amplitude spectra (C, D). Residual track noises that were removed by quadrant-swapping method were shown in E and F.

fuse spectral signature where the line noise-contaminated components are smeared out in a fan-shaped region about the mean straight line orientation of the survey tracks. However, orbits in the two data sets are essentially subparallel, and thus track-line noise for the dusk and dawn data sets are confined essentially to the symmetric pairs of odd and even numbered quadrants, respectively. Hence the noise-contaminated quadrants were simply exchanged in one of the data

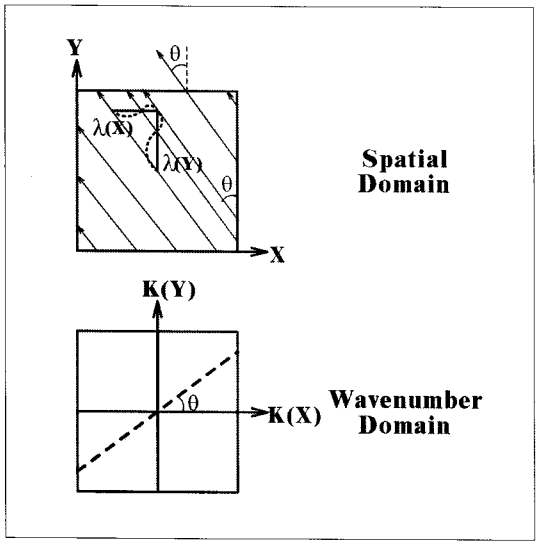

Fig. 7. Track-line noise geometries in the spatial domain (upper, and corresponding amplitude spectrum (lower) where distortions of wavenumbers are concentrated in the fan-shaped region that is centered about the heavy dashed line.

sets for the cleaner quadrants to construct a spectrum where these effects are severely attenuated. Inverse transforming the reconstructed spectrum results in total field (TF) Magsat magnetic anomalies, as shown in Fig. 8A, that are basically free of track-line noise. The track-line effects that were removed by this procedure are shown Fig. 6E and 6F, where the TF anomalies were subtracted from the maps in Fig. 6A and 6B, respectively.

To minimize distortions between satellite magnetic anomalies and their geological sources caused by corefield variations over the study area, the data were differentially-reduced-to-the-pole (DRTP). Reducing the magnetic anomalies to vertical polarization enhances the ability to relate them to geological features and reduces ambiguities in interpretation. In general, lithospheric sources of satellite magnetic anomalies may have both inductive and remanent components of magnetization. These sources may be predominantly in the lower crust that is believed to be substantially more magnetic than the upper crust (Wasilewski *et al.*, 1979: Mayhew *et al.*, 1985: Wasilewski and Mayhew, 1992). As crustal depth increases, conditions for coherent regional magnetization are enhanced. Remanence and thermal overprints are diminished, and viscous magnetization and initial susceptibility are enhanced with increasing temperature, especially within 100°C to 150°C of the Curie point. The thickness of the crust within this thermal regime of the Curie point may be 5 to 20 km depending on the steepness of the geothermal gradient. Hence, deep lithospheric mag-

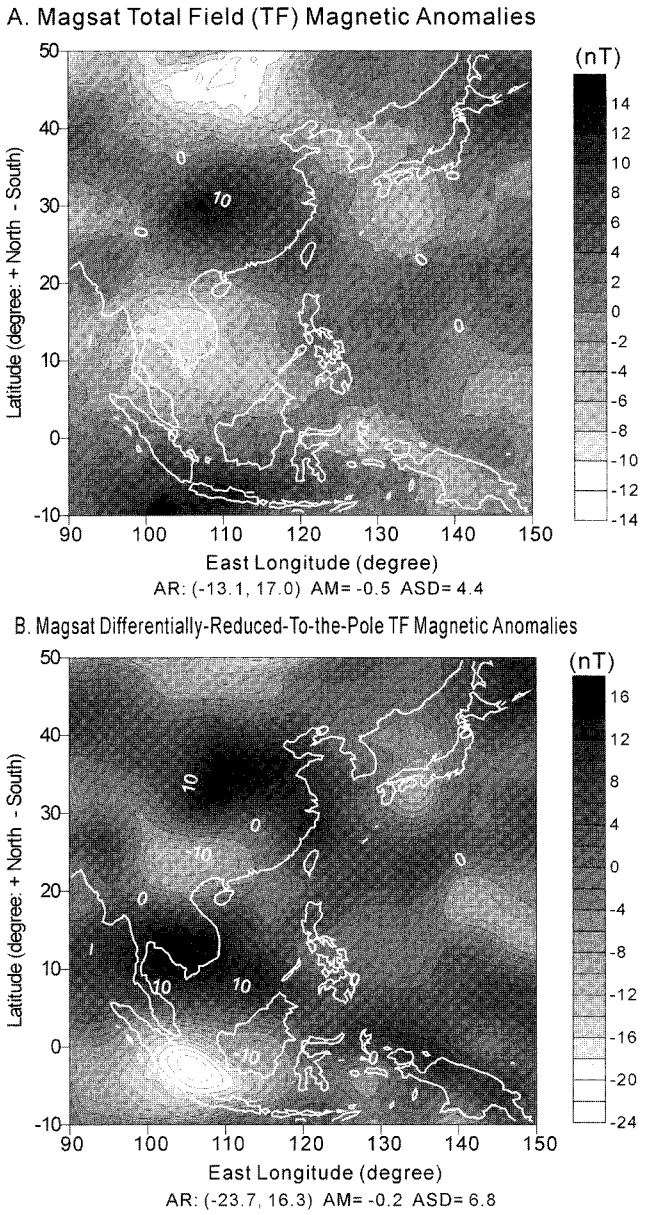

Fig. 8. Magsat total field (TF) magnetic anomalies (A) and differentially-reduced-to-the-pole TF (DRTP-TF) anomalies of East Asia (B).

netic sources are probably related to lateral variations of petrologic factors or Curie isotherm topography. Viscous remanent magnetization in the lower crust is in-phase with the induced component, so that reducing the magnetic anomalies from deep crustal sources to vertical polarization is warranted.

To differentially reduce the Magsat scalar TF magnetic anomalies in the upper panel of Fig. 8 to the pole, a set of point source magnetizations at a 2°-by-2° spacing was calculated by a least squares matrix inversion (von Frese *et al.*, 1981a). Recomputing the effects of this model using a

polarization field of inclination of 90° and intensity of 60,000 nT produces the DRTP-TF map shown in the lower panel of Fig. 8.

However, the magnetic inclination ranges between -40.8° and 68.4° in the study area, and the zero inclination is apparent almost parallel to the latitude of 10° N as shown in Fig. 3. This may result in serious distortions in the process of reduced-to-the-pole for the observations that were originally made in the two different levels (*i.e.*, airborne and spaceborne), and, hence, the Magsat TF anomalies were directly compared with the aeromagnetic anomalies in this study.

Coreelation with Aeromagnetic Anomalies

Aeromagnetic anomalies of the East Asia are correlated with Magsat magnetic anomalies at the satellite altitude, *i.e.*, 400 km, to test the lithospheric veracity of anomalies in these two data sets. The correlation analysis not only helps geologic interpretation of the data sets, but also can provide basic information for identifying lithospheric magnetic anomalies of the study area that should be common to both data sets at a common altitude. In addition to providing a good standard to judge the lithospheric integrity of the data sets, this correlation analysis may also yield a better understanding of the regional geology of East Asia.

For this correlation analysis, aeromagnetic anomaly map of East Asia 1:4,000,000 (CD-ROM Version) published by Geological Survey of Japan and CCOP (1996) was used in this paper. The CD-ROM provides both maps and anomaly data in the digital forms. In this study, the original 2-km interval data in the geographical coordinates were gridded using minimum curvature algorithm (Smith and Wessel, 1990) with a 0.125°-by-0.125° grid interval. The result is shown in Fig. 9A.

This map, however, cannot be correlated with the Magsat TF magnetic anomalies shown in Fig. 8A because they were compiled at different altitudes. The airborne anomalies were compiled at almost sea level and the spaceborne Magsat anomalies were compiled at 400 km elevation. Therefore, the airborne anomalies were low-pass filtered (LPF'd) until the map produced anomaly features that may be shown at the satellite altitude of 400 km above sea level. The LPF was spectrally done using a FFT. In other words, these smoothed anomalies were low-pass filtered for wavelengths 1.5° and greater to eliminate high frequency components that may not be shown at the satellite altitude. For a better

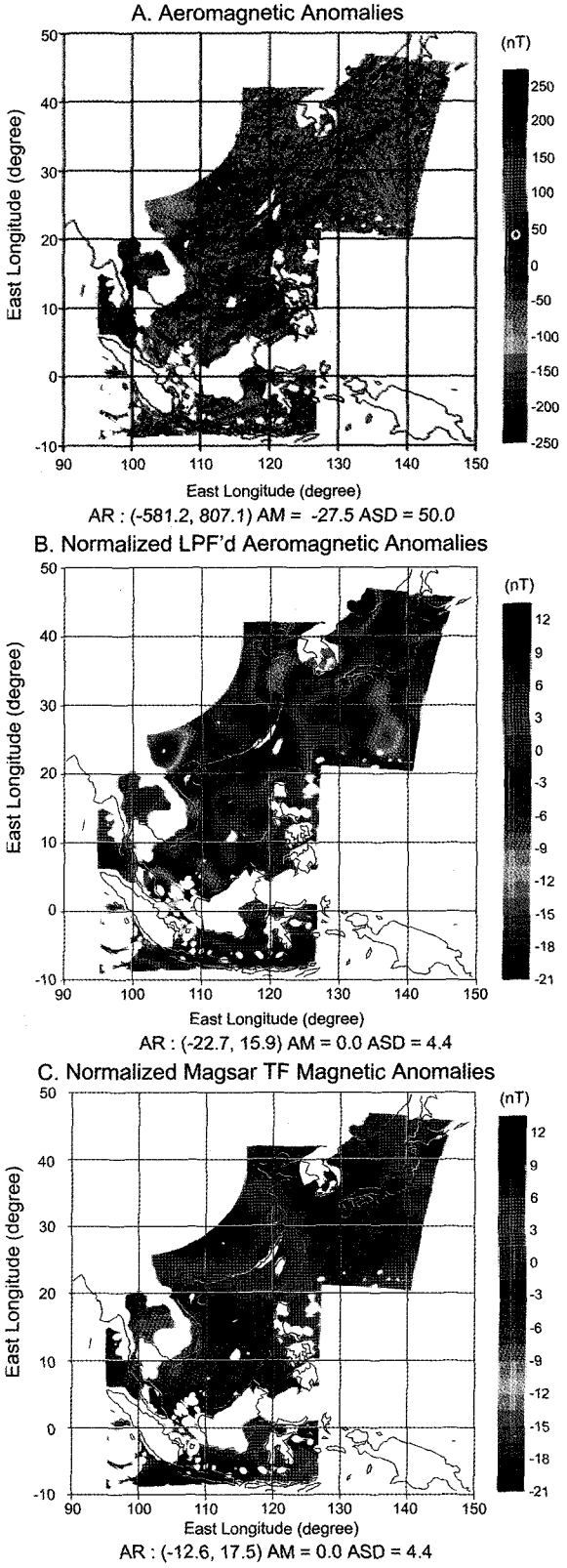

Fig. 9. A: Aeromagnetic anomalies by Geological Survey of Japan and CCOP (1996). B: Normalized low-pass filtered aeromagnetic anomalies. C: Normalized Magsat total field magnetic anomalies of East Asia. Low-Pass filtered and Magsat anomalies were normalized for graphic correlation.

graphic correlation, the LPF'd aeromagnetic anomalies were normalized to Magsat TF magnetic anomalies in Fig 8A. As a result, the two maps, shown in Fig. 9B and 9C, have now zero means and same standard deviations of 4.4.

Ideally, most features in the two maps should be directly correlated because they have common lithospheric sources. But, the CC between the two maps is only 0.243. This low CC was also found in another similar analysis (Kim, 1996: Kim *et al.*, 1995a, 1995b). The small CC between does not necessarily mean that there are not many directly correlative components in two data sets, as discussed in the paper by von Frese *et al.* (1997a, 1997b). Directly correlative Magsat and aeromagnetic anomalies are found over the Korean Peninsula and south west of Japan (trough-to-trough), which were divided by positive anomalies over the Korean. Peak-to-peak anomalies were also found over Indonesia, South China and Taiwan and surrounding seas, while inversely correlative anomalies are found over Indochina and Thailand. However, it is very difficult to discriminate directly, inversely, and nully correlative features in these two anomaly maps because features are so complicated. A spectral correlation technique, therefore, should be implemented to correlate complicated anomalies, which is beyond the scope of this paper. In general, the low CC of 0.243 between the two maps was generated by the combination of directly- and inversely-correlative anomaly features between the two maps.

Conclusions and Discussions

Improved procedures were implemented in the production of the lithospheric magnetic anomaly map from Magsat satellite magnetometer data of East Asia between 90°E-150°E and 10°S-50°N. These procedures included a more effective selection of the dusk and dawn tracks, ring current correction, and separation of core field and external field effects. External field reductions included an ionospheric correction and pass-by-pass (1-D WCA) correlation analysis. Track-line noise effects were reduced by spectral reconstruction of the dusk and dawn data sets (Kim *et al.*, 1998). The total field magnetic anomalies (Fig. 8A) were differentially-reduced-to-the-pole to minimize distortions between satellite magnetic anomalies and their geological sources caused by corefield variations over the study area (Fig. 8B). The two maps can be used for regional geology and tectonic analysis.

Aeromagnetic anomalies of the East Asia were correlated with Magsat magnetic anomalies at the satellite altitude to test the lithospheric veracity of anomalies in these two data sets. The Aeromagnetic anomalies were low-pass filtered for wavelengths 1.5° and greater to eliminate high frequency components that may not be shown at the satellite altitude. For better correlation analysis, the LPF'd aeromagnetic and Magsat maps were normalized and shown in Fig. 9B and 9C. Although the two maps have a low CC of 0.243, there are many features that are directly correlated (peak-to-peak and trough-to-trough). The low CC between the two maps was generated by the combination of directly- and inversely-correlative anomaly features between the two maps.

In general, it is very difficult to discriminate directly, inversely, and nully correlative features in these two anomaly maps because features are complicatedly correlated due to the depth and superposition of the anomaly sources. A spectral correlation technique, therefore, should be implemented to correlate complicated anomalies, which is beyond the scope of this paper. The lithospheric magnetic components were recovered successfully from satellite magnetometer observations and correlated well with aeromagnetic anomalies in this paper.

Acknowledgments

This work was supported by grant No. 2001-041-D00259 from the Korea Research Foundation.

References

Achache J., A. Abtout, and J. L. Mouel, 1987, the Downward Countinuation of the Magsat Crustal Anomaly Field over Southeast Asia: *J. Geophys. Res.*, **92**(B11), 11584-11596.

Alsdorf, D. E., R. R. B. von Frese, J. Arkani-Hamed, and H. Noltimier, 1994a, Separation of lithospheric, external, and core components of the polar geomagnetic field at satellite altitude: *J. Geophys. Res.*, **99**, 4655-4667.

Alsdorf, D. E., R. R. B. von Frese, and the Geodynamic Branch, 1994b, Fortran programs to process Magsat data for lithospheric, external field, and residual core components, NASA Technical Memorandum 104612, Goddard Space Flight Center, Greenbelt, Maryland.

Arkani-Hamed and D. W. Strangway, 1986, Effective magnetic susceptibility anomalies of the oceanic upper mantle derived from Magsat data: *J. Geophys. Res.*

Arkani-Hamed, J., S. K. Zhao, and D. W. Strangway, 1988, Geophysical interpretation of the magnetic anomalies of China derived from Magsat data: **95**, 347-359.

Cain, J. C., Z. Wang, C. Kluth, and D. R. Schmitz, 1989, Derivation of a geomagnetic model to n=63: *Geophys. J.*, **97**,

431-441.

Cohen, Y. and J. Achache, 1990, New global vector magnetic anomaly maps dericed from Magsat data: *J. Geophys. Res.*, **95**, 10783-10800.

Geological Survey of Japan and CCOP, 1996, Magnetic anomaly map of East Asia 1: 4,000,000, CD-Rom Version, Geological Survey of Japan.

Goyal, H. K., R. R. B. von Frese, W. J. Hinze, and D. N. Ravat, 1990, Statistical prediction of satellite magnetic anomalies: *Geophys. J. Int.*, **109**, 101-111.

Kim, J. W., 1996, Spectral correlation of satellite and airborne geopotential field measurements for lithospheric analysis, Ph.D. Dissertation (unpubl.), Dept. of Geological Sciences, The Ohio State University: 171p.

Kim, J. W., P. T. Taylor, and R. R. B. von Frese, 1992, Lithospheric Magnetic Anomalies of the Arabian Plate: *EOS (Am. Geophys. Union Trans.)*, **73**(43), p. 140.

Kim, J. W., R. R. B. von Frese, P. T. Taylor, and D. N. Ravat, 1994, Lithospheric Modeling of Regional Magnetic and Gravity Anomalies of the Arabian Plate: *EOS (Am. Geophys. Union Trans.)*, **75**(16), p. 131.

Kim, J. W., J.-H. Kim, R. R. B. von Frese, D. R. Roman, and K. C. Jezek, 1998, Spectral attenuation of track-line noise: *Geophys. Res. Lett*, **25**(2), p. 187-190.

Kim, J. W., R. R. B. von Frese, and P. T. Taylor, 1995a, Comparison of Satellite and Airborne Magnetic Anomalies Over the Russian Arctic: *EOS (Am. Geophys. Union Trans.)*, **76**(17), p. 273-274.

Kim, J. W., R. R. B. von Frese, P. T. Taylor, and I. C. F. Stewart, 1995b, Satellite and Aeromagnetic Anomaly Data Over the Saudi Arabian Plate: A Comparison and Interpretation, International Union of Geodesy and Geophysics: *XXI General Assembly (Boulder, CO)*, Abstracts: v.B, p. B79.

Kim, J. W., W. K. Kim, and H.-Y. Kim, 2000, Wavenumber correlation analysis of geopotential anomalies: *J. Korea Econ. Environ. Geol.*, **33**(2), p. 111-116.

Langel, R. A., J. Berbert, T. Jennings, and R. Horner, 1981, Magsat data processing: A report for Investigators, NASA Technical Memorandum 82160, Goddard Space Flight Center, Greenbelt, Maryland.

Langel, R. A., 1985, Introduction to the special issue: A perspective on Magsat results: *J. Geophys. Res.*, **90**(B3), p. 2441-2444.

Langel, R. A. and R. E. Sweeney, 1971, Asymmetric ring current at twilight local time: *J. Geophys. Res.*, **76**(19), p. 4420-4427.

Langel, R. A. and R. H. Estes, 1985, The near-earth geomagnetic field at 1980 determined from Magsat data: *J. Geophys. Res.*, **90**, 2495-2510.

Mayhew, M. A., 1985, Curie Isotherm Surface Inferred From High-Altitude Magnetic Anomaly Data: *J. Geophys. Res.*, **90**, 2647-2654.

Meyer, J., J. H. Hufer, M. Siebert, and A. Hahn, 1985, On the identification of Magsat anomaly charts as crustal part of internal field: *J. Geophys. Res.*, **90**, 2537-2542.

Potemra, R. A., F. F. Mobley, and L. D. Exkard, 1980, The geomagnetic field and its measurement: Introduction and Magnetic Field Satellite (Magsat) glossary: *Johns Hopkins APL Technical Digest*, **1**(3), p. 162-170.

Ravat, D. and W. J. Hinze, 1993, Consideration of Varations in Ionospheric Field Effects in Mapping Equatorial Lithospheric Magsat Magnetic Anomalies: *Geophys. J. Int.*

Regan, R. D., J. C. Cain, and W. M. Davis, 1975, A global magnetic anomaly map: *J. Geophys. Res.*, **80**, 794-802.

Smith, W. H. F. and P. Wessel, 1990 Gridding with continuous curvature splines in tension: *Geophysics*, **55**, 293-305.

von Frese, R. R. B., W. J. Hinze, C. A. McGue, and D. N. Ravat, 1989, Use of satellite magnetic anomalies for tectonic lineament studies: *Memoirs Geological Society of India*, **12**, 171-180.

von Frese, R. R. B., M. B. Jones, J. W. Kim, and J.-H. Kim, 1997a, Analysis of anomaly correlations: *Geophysics*, **62**(1), p. 342-351.

von Frese, R. R. B., M. B. Jones, J. W. Kim, and W. S. Li, 1997b, Spectral correlation of magnetic and gravity anomalies of Ohio: *Geophysics*, **62**(1), p. 365-380.

Wasilewski, P. J., H. H. Thomas, and M. A. Mayhew, 1979, The Moho as a magnetic boundary: *Geophys. Res. Lett.*, **6**, 541-544.

Wasilewski, P. J. and M. A. Mayhew, 1992, The Moho as a Magnetic Boundary Revisited: *Geophys. Res. Lett.*, **19**(22), 2259-2262.

Yanagisawa, M. and M. Kono, 1985, Mean ionospheric field correction for Magsat data: *J. Geophys. Res.*, **90**, 2527-2536.